

9315  
8006 NT AVAN

TECH LIBRARY KAFB, NM  
0066127

# NATIONAL ADVISORY COMMITTEE FOR AERONAUTICS

TECHNICAL NOTE 3008

EFFECTS OF FINITE SPAN ON THE SECTION CHARACTERISTICS  
OF TWO 45° SWEEPBACK WINGS OF ASPECT RATIO 6

By Lynn W. Hunton

Ames Aeronautical Laboratory  
Moffett Field, Calif.



Washington  
September 1953

AFMDC  
TECHNICAL LIBRARY  
AFL 2311



---

TECHNICAL NOTE 3008

---

## EFFECTS OF FINITE SPAN ON THE SECTION CHARACTERISTICS

## OF TWO 45° SWEEPBACK WINGS OF ASPECT RATIO 6

By Lynn W. Hunton

## SUMMARY

A study of the finite-span effects on the local loading characteristics of two sweptback wings at low speed has been made with a view toward providing some insight into the usefulness of two-dimensional section data and span-loading theory for determining the characteristics of sections of a swept wing. The two wings considered, for which complete pressure-distribution data were available at large scale, were identical in plan form having 45° of sweepback and an aspect ratio of 6 and differed in twist and in sections, the latter being the NACA 64A010 and NACA 64A810.

At low values of lift coefficient, the finite-span effects are restricted to regions of the wing close to the root and tip. At higher values of lift a three-dimensional viscous effect becomes evident. Examination of this effect reveals that the lateral flow of the boundary-layer air acts as a boundary-layer-control agent over virtually the entire span of the wing, alleviating flow separation and thus increasing the local maximum lift coefficient beyond that expected of the section in two-dimensional oblique flow. The effect is greatest near the root, diminishing gradually spanwise in approaching the tip. Near the tip where there is little boundary-layer-control effect the local section characteristics closely resemble those for the two-dimensional section in oblique flow.

## INTRODUCTION

For unswept wings it has been recognized for some time that the three-dimensional effects introduced by the finite span could be successfully isolated to the span-loading characteristics and that the characteristics of any one section of the wing could be related to two-dimensional results (e.g., refs. 1 and 2). Thus, a reliable span-loading theory used in conjunction with two-dimensional section data affords a simple procedure for determining surface loadings on the unswept wing. The design of swept wings likewise would be greatly facilitated if an equally simple and effective procedure for determining surface loadings were available. Simplified lifting-surface theory has been shown to give reliable indications of plan-form effects, including sweep, on span loading as long as no separation exists (ref. 3). For chordwise loadings

simple sweep theory has been proven valid for the case of a two-dimensional section in yawed flow (ref. 4). It would appear, therefore, that on the swept wing it should be possible to separate, at least to a degree, plan-form and section characteristics by a means similar to that in use for the straight wing. The applicability of such a procedure to the swept wing, of course, hinges on the extent to which the chordwise loadings are influenced by the three-dimensional effects.

Pressure-distribution measurements have been made at low speed for two large-scale  $45^\circ$  sweptback wings having identical plan forms but different section profiles and markedly dissimilar stalling characteristics. On the basis of these loadings, an attempt will be made to show for these two sweptback wings, first, the magnitude of three-dimensional effects on the local section loadings through analysis of section pressure diagrams and, second, the suitability of the procedure (two-dimensional data combined with span-loading theory) for application to either the linear or nonlinear lift ranges through examination of local section lift curves.

#### NOTATION

$C_L$	lift coefficient, $\frac{\text{lift}}{qS}$
$C_D$	drag coefficient, $\frac{\text{drag}}{qS}$
$C_m$	pitching-moment coefficient, $\frac{\text{pitching moment}}{qS\bar{c}}$
$P$	pressure coefficient, $\frac{P_l - P}{q}$
$c_l$	section lift coefficient, $\frac{\text{section lift}}{qc}$
$R$	Reynolds number based on $\bar{c}$
$S$	area of semispan wing, sq ft
$b$	span of complete wing, ft
$c$	local chord measured parallel to plane of symmetry, ft

$\bar{c}$	wing mean aerodynamic chord, $\frac{\int_0^{b/2} c^2 dy}{\int_0^{b/2} c dy}$ , ft
q	free-stream dynamic pressure, lb/sq ft
p	free-stream static pressure, lb/sq ft
$p_l$	local static pressure, lb/sq ft
c.p.	center of pressure, percent chord
$\alpha$	angle of attack of wing-root section, deg
$\alpha_0$	angle of attack for two-dimensional airfoils, deg
$\alpha_{L_0}$	wing zero-lift angle of attack, deg
$\alpha_{l_0}$	section zero-lift angle of attack, deg
$\alpha_r$	angle of attack of wing-root section for zero net lift on the wing for loading associated with wing twist, deg
$\epsilon$	angle of twist with respect to root chord (positive for washin), deg
$\eta$	fraction of semispan
$\Lambda$	sweep angle of the wing quarter-chord line, deg

## Subscripts

t.e.sep	trailing-edge separation
max	maximum
$\Lambda$	yawed flow

## MODELS AND APPARATUS

Pertinent dimensions of the two wing-fuselage models are given in figure 1. The wings were identical in plan form, having  $45^\circ$  of sweep-back of the quarter-chord line, an aspect ratio of 6, and a taper ratio of 0.5. One wing was uncambered and untwisted, henceforth called the plain wing, and employed an NACA 64A010 airfoil section normal to the quarter-chord line. The second wing, henceforth called the cambered, twisted wing, had  $10^\circ$  washout of the tip (see fig. 1 for twist distribution) and employed an NACA 64A810,  $a = 0.8$  (modified) airfoil section normal to the quarter-chord line. Each wing was equipped with six rows of static-pressure orifices as indicated in figure 1. Tests of the wing-fuselage models were conducted in the Ames 40- by 80-foot wind tunnel with the models mounted vertically on the test-section floor in a semi-span type of installation.

The two-dimensional test models of the NACA 64A010 and 64A810,  $a = 0.8$  (modified), airfoils were 3-1/2 and 4 feet in length of chord, respectively. These tests were conducted in the Ames 7- by 10-foot wind tunnel with the models spanning the 7-foot dimension. A row of static-pressure orifices was located at the midspans of both section models.

## RESULTS AND DISCUSSION

Pressure data obtained on two large-scale sweptback wings, identical in plan-form geometry but dissimilar in stalling behavior, have been analyzed in an attempt to gain some insight into the nature and extent of the influence of finite-span effects on local section loadings. The dissimilarity in stalling behavior between the two models was attributable principally to a difference in section profile; the section of one wing was symmetrical (NACA 64A010) and the other was highly cambered (NACA 64A810). Two-dimensional tests reported in reference 5 showed the 64A010 airfoil to stall from leading-edge flow separation; whereas those reported in reference 6 showed the 64A810 airfoil to stall primarily from turbulent separation near the trailing edge. For reference purposes three-component force data for the two wing-fuselage models are presented in figure 2 while in figure 3 are given the lift characteristics<sup>1</sup> of the two airfoil sections. All wing data presented throughout the report were obtained at a Mach number of 0.2 and a Reynolds number of 8 million based on the mean aerodynamic chord of 6.21 feet. All two-dimensional data are given for a Reynolds number of 4.1 and 3.7 million

---

<sup>1</sup>The lift curve for the NACA 64A010 section was obtained from the aerodynamic data of reference 7 since the data of reference 5 are uncorrected for tunnel-wall effects.

---

for the uncambered and cambered sections, respectively; these values correspond closely with the average effective Reynolds number of 4 million for the wings based on the components of the mean aerodynamic chord and velocity both taken normal to the wing quarter-chord line.

For purposes of this investigation, the general study of the influence of three-dimensional effects on the local loading characteristics of the swept wings is divided into two parts. In the first part an attempt is made to isolate the influence of three-dimensional effects on the local chordwise distribution of loading at a number of semispan stations. The analysis for this case consists of comparisons of two-dimensional pressure distributions with the local pressure distributions measured on the wing models, the comparisons being made in most cases on an equal lift coefficient basis (i.e., equal pressure diagram area). These results are presented in figures 4 and 5 for the plain and cambered, twisted wings, respectively. For additional clarification of this phase of the study there are also given local center-of-pressure results in figure 6 and variation spanwise of local  $c_{l_{max}}$  for both wings in figure 7.

The second part of the analysis is directed at demonstrating the extent to which local lift values on the swept wing can be determined for conditions involving either unseparated or separated flow. For this purpose local lift curves derived for several semispan stations of the swept wings from two-dimensional experimental data and Weissinger span-loading theory are correlated with the local lift curves measured on the wing models. These results are shown in figure 8.

#### Local Pressure-Distribution Comparisons

The local pressure-distribution curves in figures 4 and 5 are shown for six semispan stations of both wing models. Four of these stations (see fig. 1) were oriented normal to the wing quarter-chord line following the concept of simple sweep theory. However, in order to determine the three-dimensional influence on the loadings close to the root and tip, it was necessary to orient the orifice stations in these two regions parallel to the free-stream direction.<sup>2</sup> The pressure data for each of these wings are given for a range of lift-coefficient values extending to beyond stall.

---

<sup>2</sup>Taper introduces a variation in the location percentagewise of pressure orifices depending on the reference chord used. Herein the pressure data in each case are given with respect to the chord line defined by the particular arrangement of pressure orifices. For these wings with moderate taper the consequent departure from the basic simple sweep concept in the case of the two streamwise stations is small and has been neglected.

---

The accuracy of the simple theory of sweep for defining the effect of sweep on the pressure distribution of a two-dimensional section at moderate angles of attack is generally accepted. Demonstrations of this accuracy have been shown in a number of two-dimensional tests, one of which is reported in reference 4. A comparison of pressure distributions derived from this two-dimensional theory with those measured on the finite-span wing thus should give a quantitative measure of the degree to which the local section loading characteristics are influenced by three-dimensional effects. There arises then the question as to a definition of the effective section of the finite wing with taper for which a variation in sweep angle of the constant percent chord lines is involved. Theoretical considerations would indicate such a section to be normal to the lines of constant percent chord at all points. Obviously, such a section would be curved which would entail a variation chordwise in the effective potential velocity. For purposes of this study such a refinement was deemed unnecessary and instead an average straight-line section normal to the quarter-chord line was employed. Accordingly, the two-dimensional pressure diagrams used in the analysis for comparison with the local pressure distributions measured on the wing, streamwise and chordwise station data alike, are based on the NACA 64A010 section for the plain wing and the NACA 64A810 section for the cambered, twisted wing and in each case are computed for the same value of local  $c_l$  as that measured on the wing. These pressures were derived on the basis of simple sweep theory, that is, pressure-coefficient values were interpolated from unyawed two-dimensional data for values of

$$c_{l_{\Lambda=0}} = \frac{c_{l(\text{wing})}}{\cos^2 \Lambda}$$

To be applicable to the swept wing, the values of pressure coefficient so determined for the foregoing values of  $c_{l_{\Lambda=0}}$  then were converted to yawed flow, thus

$$P_{\Lambda} = P_{\Lambda=0} \times \cos^2 \Lambda$$

Comparisons of theoretical pressure distributions with the two- and three-dimensional data are also included in most of the figures. These values were derived by the method of velocity superposition described in reference 8 and converted to yawed flow following the procedure outlined for the two-dimensional-data case.

Plain wing.- Inspection of figure 4 reveals that the correlation of pressures for the finite wing with those for the yawed infinite span section is generally quite close at most stations for lift coefficients ranging to 0.6. This lift range corresponds to that for

which little or no separation could be detected from the pressure distributions on the wing. The most obvious deviation in these pressure comparisons appears near the root at stations 0.167 and 0.383. At zero lift (fig. 4(a)) some possible evidence of the induced velocity effect on the base profile pressure distribution<sup>3</sup> resulting in a shift rearward of the minimum pressure point appears at station 0.167 while at station 0.383 and at the tip station 0.924 virtually no influence of this effect may be seen. The general rise in level of the pressures at stations 0.167 and 0.383 is attributable to interference of the fuselage; this effect, however, being fairly uniform over the chord, does not materially alter the distributions of local loading. With introduction of additional type lift, an induced camber effect<sup>4</sup> appears in the results of figure 6 as a shift in the center of pressure of 4-percent chord rearward at the root station and 3-percent chord forward at the tip station with virtually no effect appearing at the intermediate stations. Despite indications of theory where induced camber is proportional to  $C_L$ , what effect does appear in these results is almost constant for lift coefficients above 0.2. Hence, from these results in the lift range involving no flow separation, it may be deduced that (1) the influence of the finite span resolves into only one significant effect, that of induced camber which is concentrated quite close to the wing-fuselage juncture and the tip, and (2) over the remaining major proportion of the exposed wing span the chordwise load distributions for all practical purposes behave like the infinite span section in oblique flow.

From the pressure data for this wing it was found that initial stall resulted from flow separation near the leading edge of tip stations at a  $C_L$  of 0.65. In figure 4(d) it may be seen that just prior to flow separation at a  $C_L$  of 0.60, all stations of the wing but one (0.924) have exceeded the two-dimensional value of  $c_{l_{max}}$  corrected for sweep ( $1.10 \times \cos^2 45^\circ = 0.55$ ). For these cases it was not possible to match pressure diagram areas; instead, the pressure distribution from two-dimensional tests is shown for the NACA 64A010 section just over stall at an indicated  $c_l$  of 0.41 (in oblique flow). The theoretical pressure distributions on the other hand match closely the wing pressures just prior to stall at all stations except near the fuselage juncture. In the theoretical pressure distributions there is, of course, no account taken of the viscous effects. The close correlations so shown then must be an indication that little or no separation was present prior to wing stall even though the two-dimensional  $c_{l_{max}}$  has been exceeded at most points. This delay in separation and consequent increase in the value of local  $c_{l_{max}}$  as compared to the yawed infinite span section  $c_{l_{max}}$  of 0.55 is illustrated in figure 7. Near the tip the two-dimensional and wing values agree closely, whereas progressing inboard the wing local  $c_{l_{max}}$  values increase to almost three times the two-dimensional value in yawed flow. This result thus clearly demonstrates the action of the major three-dimensional effect present on the swept wing when separation

---

<sup>3</sup>See references 9 and 10 for theoretical treatment of this effect.

<sup>4</sup>See reference 11.

---

is either imminent or has occurred; namely, the influence of the three-dimensional boundary-layer-control effect afforded by lateral flow of boundary-layer air. The consequences are greatest near the root diminishing to almost no effect at the tip. A lack of means to evaluate this effect for any plan form represents, at the present time, the major obstacle preventing accurate predictions to be made of the characteristics of swept wings.

In view of the significant increases in the local  $c_{l_{max}}$  values brought about by the three-dimensional boundary-layer characteristics, it is of interest to consider the stalling behavior of these sections to see what changes occurred. Comparisons of the two-dimensional and wing-pressure distributions following stall are given in figure 4(e). Each pressure diagram shown corresponds to the first evidence of a loss in nose peak pressures at the particular station except that at the root station 0.167 where stall was never reached. Also included are the values of wing  $C_L$  for which the data at each station are given. The variation shown in wing  $C_L$  for each station is indicative of the progression of stall from the tip to the root. The stall of the NACA 64A010 section was described in reference 5 to be of the type where the flow separated near the leading edge but reattached at about the 15-percent-chord point, causing partial recovery of the free-stream pressure from this point to the trailing edge. On the wing the mechanism of flow separation at most stations appears to be quite similar to the observed characteristics for the two-dimensional section. However, the point of reattachment of flow on the wing sections is much closer to the leading edge and the pressure-recovery gradient supported by the three-dimensional flow conditions is somewhat steeper than that exhibited by the two-dimensional section.

Cambered, twisted wing.- The pressure-distribution comparisons for the cambered, twisted wing in figure 5 are given for a wing lift-coefficient range extending from 0.15 to just beyond the  $C_{L_{max}}$  of 1.09. As briefly mentioned earlier, the characteristics of this wing are influenced strongly by turbulent separation. Two-dimensional tests of the NACA 64A810 airfoil showed that turbulent separation began at a  $c_l$  of 1.06. For the section yawed  $45^\circ$ , then, such separation would be anticipated at a  $c_l$  of 0.53 ( $1.06 \times \cos^2 45^\circ$ ). This  $c_l$  value is reached locally on the wing first at the inboard stations at a wing  $C_L$  of about 0.50. The comparisons of pressure distributions given for lift coefficients of 0.15 and 0.50 show quite close agreement except for the root and tip effects. These effects appear similar to and of roughly the same magnitude as those discussed for the plain wing. The only difference to be noted (fig. 6) is an unexplained failure of the center of pressure at the root station to shift rearward as would be indicated by theory and as the plain wing showed.

Above a wing  $C_L$  of 0.50 the two-dimensional pressure distributions begin to show a noticeable deviation from the inboard station loadings, these stations having reached values of  $c_l$  over 0.53.

Above this, the two-dimensional pressures exhibit trailing-edge separation whereas the inboard station wing pressures show no separation and hence continue to match closely the theoretical pressure distributions. At a  $C_L$  of 0.83, however, the local loading near the tip (0.924) exceeded a  $c_l$  of 0.53 at which time turbulent separation began on the wing, quickly spreading inboard from this point. This variation spanwise in the  $c_l$  value for incidence of turbulent separation is shown in figure 7. Near the root turbulent separation never developed, while conditions near the tip match closely the two-dimensional characteristics. Hence it is seen that, owing to boundary-layer control resulting from the lateral flow of boundary-layer air, trailing-edge separation was delayed over most of the wing until such time as a section near the tip reached the two-dimensional value of  $c_l$  for such separation. Furthermore, since the formation and growth of separation at the outboard stations agree closely with the yawed section characteristics, it is apparent that the flow of boundary-layer air toward this region does not have a detrimental effect on the local section stalling behavior at this relatively large test Reynolds number of 8 million.

In figure 5(e) the data at a  $C_L$  of 1.01 show conditions on the wing just preceding  $C_{L_{max}}$  and complete flow breakdown which occurred at a  $C_L$  of 1.09. All stations but that at 0.924 have exceeded the  $c_{l_{max}}$  of 0.84 for the yawed two-dimensional section. The large variation in  $c_{l_{max}}$  spanwise may be seen in figure 7 where it is indicated that at the 0.38 span station an increase in  $c_{l_{max}}$  of nearly 70 percent above the two-dimensional value was measured while at the root station, although the absolute magnitude of  $c_{l_{max}}$  was not determined, indications point to a much higher percentage increase.

Comparisons of two- and three-dimensional pressure distributions beyond  $C_{L_{max}}$  at a  $C_L$  of 1.06 are given in figure 5(f). As in the case of the plain wing, the two-dimensional data are given for  $c_{l_{max}}$ , there being no attempt made to equalize the pressure diagram areas for the stalled condition. The stall of the NACA 64A810 section in two-dimensional flow occurred at  $14^\circ$  angle of attack and was gradual with little loss in lift with increase in angle of attack to  $16^\circ$ . In reference 6, this stall was described as resulting from gradual progression forward of turbulent separation with little loss in nose peak pressures being observed even beyond  $c_{l_{max}}$ . On the three-dimensional wing, however, the stall was found to be somewhat more abrupt where, with  $1^\circ$  change in angle of attack ( $21^\circ$  to  $22^\circ$ ), turbulent separation progressed forward about 0.6 chord nearly to the leading edge at outboard stations, and leading-edge separation and reattachment type of stall resulted at stations farther inboard. Thus, it is seen that the stalling characteristics of inboard sections can be completely altered, presumably by the three-dimensional boundary-layer conditions present on the sweptback wing.

## Local Lift-Curve Comparisons

The preceding section was directed at demonstrating the extent of correlation that exists between two-dimensional pressure distributions and those on the finite-span swept wing, these correlations being based on equal values of lift. Use of two-dimensional or theoretical data for prediction of chordwise loadings requires a knowledge of the local lift distribution across the span of the wing. In the lift range involving no flow separation where local lift curves generally are linear, the span-loading theory accounts quite accurately for the variation span-wise in local lift-curve slopes induced by the finite span. In the lift range where flow separation has occurred, it has been proven practical in the case of unswept wings to rely on two-dimensional test data to obtain the nonlinear lift characteristics of the local semispan sections (e.g., ref. 2). To demonstrate the adequacy of these unswept-wing procedures when applied to the swept wing at lift coefficients covering conditions involving either unseparated or separated flow, comparisons will be made of predicted and measured local-lift curves for the two models considered in the previous section. These comparisons for six semispan stations on each wing are given in figure 8.

The yawed infinite wing lift curves for the NACA 64A010 and NACA 64A810 airfoils from which the predicted local lift curves on each wing were derived are also given in figure 8. These yawed-flow curves were determined from the two-dimensional experimental lift curves of figure 3 following simple sweep theory. Thus, the angles of attack and corresponding values of lift coefficient were adjusted in the following manner:

$$\alpha_{0\Lambda} = \alpha_{0\Lambda=0} \times \cos 45^\circ$$

$$c_{l\Lambda} = c_{l\Lambda=0} \times \cos^2 45^\circ$$

Local lift curves for the various stations of each wing were then found by rocking the yawed infinite wing lift curve to the local slope given by the Weissinger span-loading method. This step was accomplished by shearing the curves holding the values of  $c_l$  constant and adjusting  $\alpha$  to give the theoretical slope, it being assumed that the deviation of the local slope from the two-dimensional value stems largely from the induced angles. The matching of local slopes to theory was restricted to just the low-lift linear range of the experimental curves. For the plain wing having symmetry, the angles of zero lift for the wing and local stations are, of course, all zero. However, for the cambered, twisted wing the angle of zero lift is a function of both the camber ( $\alpha_{l_0}$ ) and the twist ( $\alpha_r$ ). The  $\alpha_{l_0}$  of a cambered section in yawed flow reduces by the cosine of the sweep angle, while the angle of attack of the root station  $\alpha_r$  for zero lift on a twisted wing is given by the Weissinger loading method. Hence, the angle for zero lift of the wing becomes

$$\alpha_{L_0} = \alpha_{l_0} \times \cos 45^\circ + \alpha_r$$

Since the camber was constant across the span, the wing at the angle of attack for zero lift carries a basic span-lift distribution dependent only on the twist distribution. This basic lift distribution and the  $\alpha_{L_0}$  for the wing then establishes on the lift curve the coordinates of one point for each semispan station through which the various predicted local lift curves must pass.

Plain wing.- The results in figure 8(a) show that the theoretical lift-curve slopes agree very closely with experiment for all stations of the wing, thus verifying the accuracy of the span-loading theory. The  $c_{l_{max}}$  of the NACA 64A010 airfoil in a  $45^\circ$  oblique flow would be 0.55. All stations of the wing exceed this value, some by quite a wide margin as was also seen earlier in figure 7, the 0.924 station showing the closest agreement. On this wing having a section with virtually a linear lift curve to  $c_{l_{max}}$ , this variation in local  $c_{l_{max}}$  across the span, therefore, represents the principal three-dimensional effect and indicates the effectiveness of the lateral flow of the boundary-layer air as a boundary-layer-control agent.

Cambered, twisted wing.- The linear portion of the oblique-section lift curve extending to a  $c_l$  of about 0.53 was used to define the slope of the local curves. In this lift range the theoretical and experimental slopes agree closely. The predicted  $\alpha_{L_0}$  of  $-1.4^\circ$  (based on  $\alpha_{L_0}$  of  $-6.2^\circ$  and  $\alpha_T$  of  $2.9^\circ$ ), however, may be seen to deviate from experiment by approximately  $-1^\circ$ . The discrepancy possibly stems from an inaccuracy involved in assuming the span loadings due to camber and to angle of attack to be equivalent. In the upper lift range (above 0.53) where the NACA 64A810 section in oblique flow exhibited turbulent separation, these predicted curves show an increasing departure from experiment as stations near the root are approached, following the pattern fully discussed earlier in connection with the chordwise loading study. With the exception of the 0.924 station, it may be seen that all local stations of the wing exceeded the two-dimensional  $c_{l_{max}}$  in yawed flow of 0.84. The failure of the tip station to fully attain the two-dimensional  $c_{l_{max}}$ , as did the tip of the plain wing, is believed attributable to the severe washout of  $-10^\circ$ ; initial leading-edge flow separation occurred at an inboard station and contributed to the premature stalling of the tip. It would appear clear from these comparisons, therefore, that in the nonlinear lift range the three-dimensional viscous effects become so dominant that only at the outboard stations are the two-dimensional nonlinear lift characteristics even approximately simulated.

#### Evaluation of Surface-Loading Procedure

In the preceding sections the two principal steps involved in the application of two-dimensional data and span-loading theory to determining surface loadings on the swept wing have been demonstrated. In

the first section the local pressure-distribution comparisons were studied through  $C_{l_{max}}$  on the assumption that the local-lift value would be known. In the second section the applicability of a procedure for determining the local-lift values in the linear as well as nonlinear lift ranges was studied. From these results for two wings with  $45^\circ$  of sweepback it was found that the lift ranges involving unseparated or separated flow clearly marked two distinct regimes insofar as the applicability to the swept wings of two-dimensional data and span-loading theory were concerned. In the absence of flow separation, quite accurate local loadings could be determined except near the root and tip where shifts in the center of pressure to the order of 0.05 chord were measured. When flow separation became imminent, either of the laminar or turbulent type, it appeared that three-dimensional viscous forces came into play such as to delay the separation until stations near the tip (region of 0.9 semispan) reached the two-dimensional value of  $c_l$  for such separation. Whether these results are generally applicable at other Reynolds numbers is open to some question in view of the importance of viscosity in governing the characteristics of the swept wing. The results herein were obtained at a Reynolds number sufficiently large that the effective Reynolds number of the tip section normal to the quarter-chord line was above the critical range for  $c_{l_{max}}$  in two-dimensional flow.

#### CONCLUSIONS

A study has been made of the extent to which the local chordwise loading characteristics of two swept wings are determinable from yawed, infinite-span section data and span-loading theory. Directly involved in such a study was an evaluation of the influence of three-dimensional effects on the local loadings. The general conclusions reached regarding these finite-span effects for two large-scale  $45^\circ$  sweptback wings of aspect ratio 6 were as follows:

1. In the low-lift range, the finite-span effects were restricted to areas of the wing near the root and tip which, combined, affected approximately 25 percent of the span causing a deviation in local center of pressure in these two areas of 3- to 5-percent chord.

2. At the higher lift coefficients, evidence of a boundary-layer-control effect was present which presumably could be traced to the lateral flow of the boundary-layer air. Examination of this phenomenon revealed the following:

- (a) The effect tended in all cases to delay flow separation and thus increase  $c_{l_{max}}$  beyond that expected of the section in two-dimensional oblique flow.

(b) The effect was greatest near the root and diminished gradually spanwise in approaching the tip.

3. Near the tip where the boundary-layer control was a minimum, the local sections behaved much like the corresponding two-dimensional section in oblique flow. Hence, it would appear from these results that occurrence of initial stall at the tip of most sweptback wings is chargeable to increased values of  $c_{l,max}$  of inboard sections rather than to any deleterious influence of the three-dimensional viscous effects at the tip.

Ames Aeronautical Laboratory  
National Advisory Committee for Aeronautics  
Moffett Field, Calif., Jan. 10, 1952

#### REFERENCES

1. Anderson, Raymond F.: Determination of the Characteristics of Tapered Wings. NACA Rep. 572, 1936.
2. Sivells, James C., and Neely, Robert H.: Method for Calculating Wing Characteristics by Lifting-Line Theory Using Nonlinear Section Lift Data. NACA TN 1269, 1947.
3. DeYoung, John, and Harper, Charles W.: Theoretical Symmetric Span Loading at Subsonic Speeds for Wings Having Arbitrary Plan Form. NACA Rep. 921, 1948.
4. Lippisch, A., and Beuschauen, W.: Pressure Distribution Measurements at High Speed and Oblique Incidence of Flow. NACA TM 1115, 1947.
5. Peterson, Robert F.: The Boundary-Layer and Stalling Characteristics of the NACA 64A010 Airfoil Section. NACA TN 2235, 1950.
6. McCullough, George B., and Haire, William M.: Low-Speed Characteristics of Four Cambered, 10-Percent-Thick NACA Airfoil Sections. NACA TN 2177, 1950.
7. Loftin, Laurence K., Jr.: Theoretical and Experimental Data for a Number of NACA 6A-Series Airfoil Sections. NACA Rep. 903, 1948. (Formerly NACA RM L6J01, and TN 1368)
8. Abbott, Ira H., von Doenhoff, Albert E., and Stivers, Louis S., Jr.: Summary of Airfoil Data. NACA Rep. 824, 1945. (Formerly NACA ACR L5C05)

9. Jones, Robert T.: Subsonic Flow Over Thin Oblique Airfoils at Zero Lift. NACA Rep. 902, 1948. (Formerly NACA TN 1340)
10. Neumark, S.: Critical Mach Numbers for Swept-Back Wings. The Aeronautical Quarterly, August, 1950, pp. 85-110.
11. Falkner, V. M.: The Calculation of Aerodynamic Loading on Surfaces of Any Shape. R. & M. No. 1910, British A.R.C., 1943.

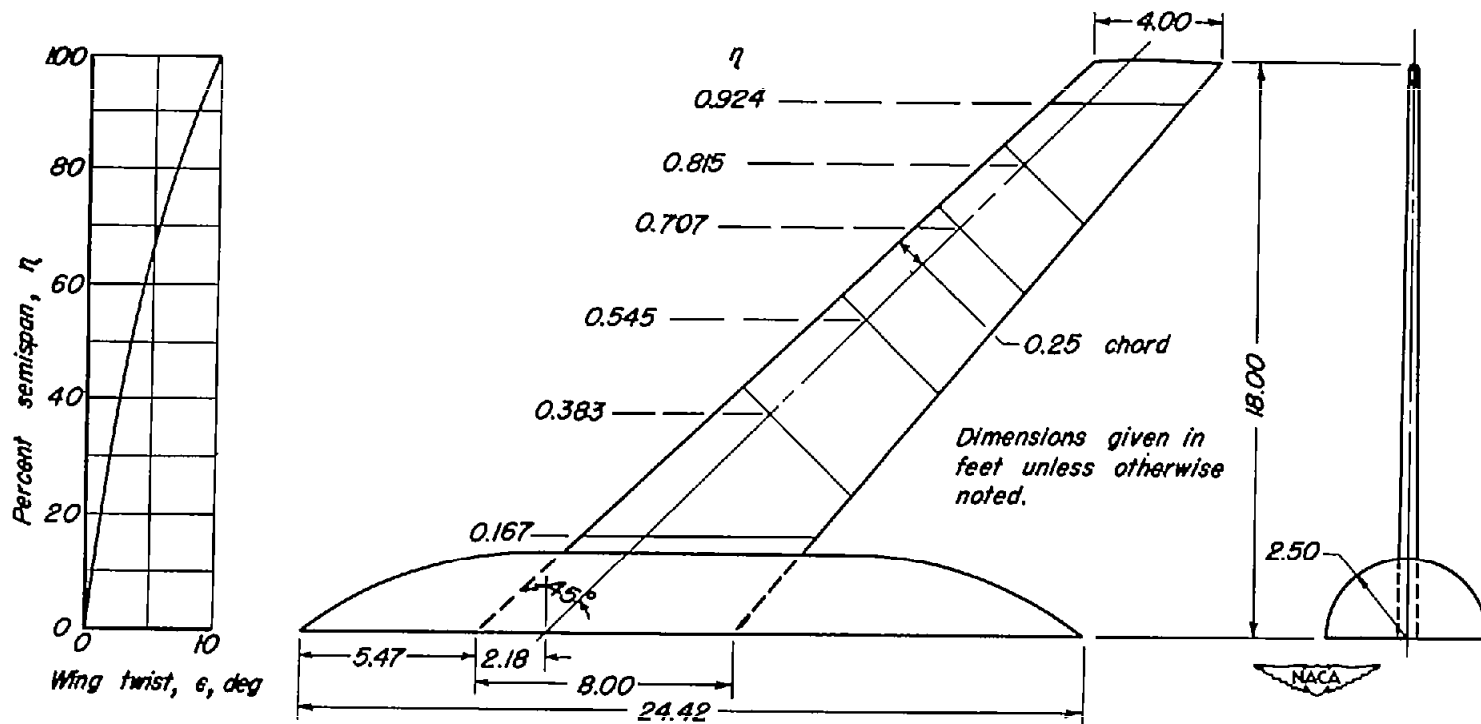


Figure 1.—Dimensions of the semispan wing-fuselage models including the orifice station locations and the twist distribution for the cambered, twisted wing.

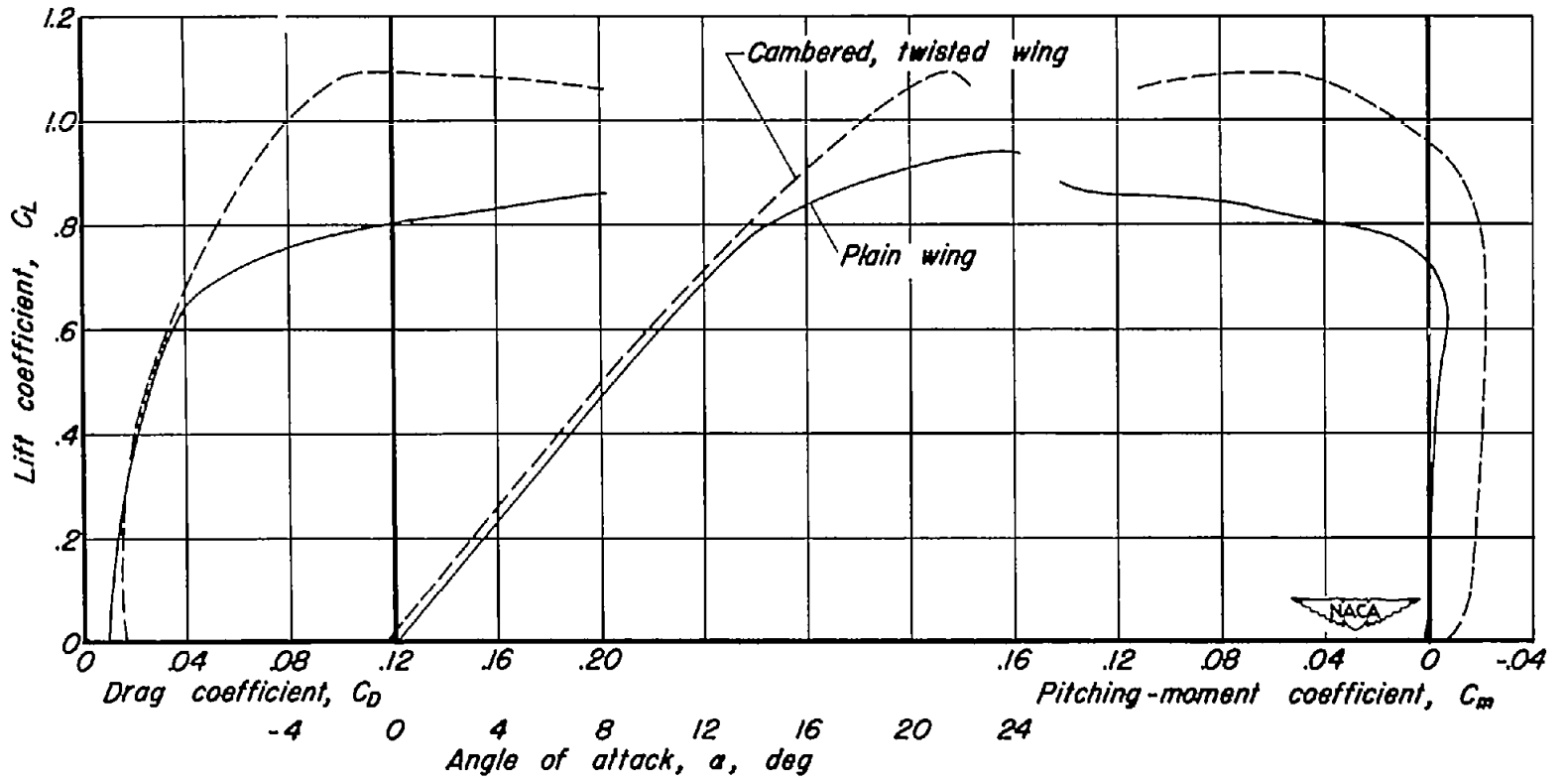


Figure 2.— Drag, lift, and pitching-moment characteristics of the two wing models.

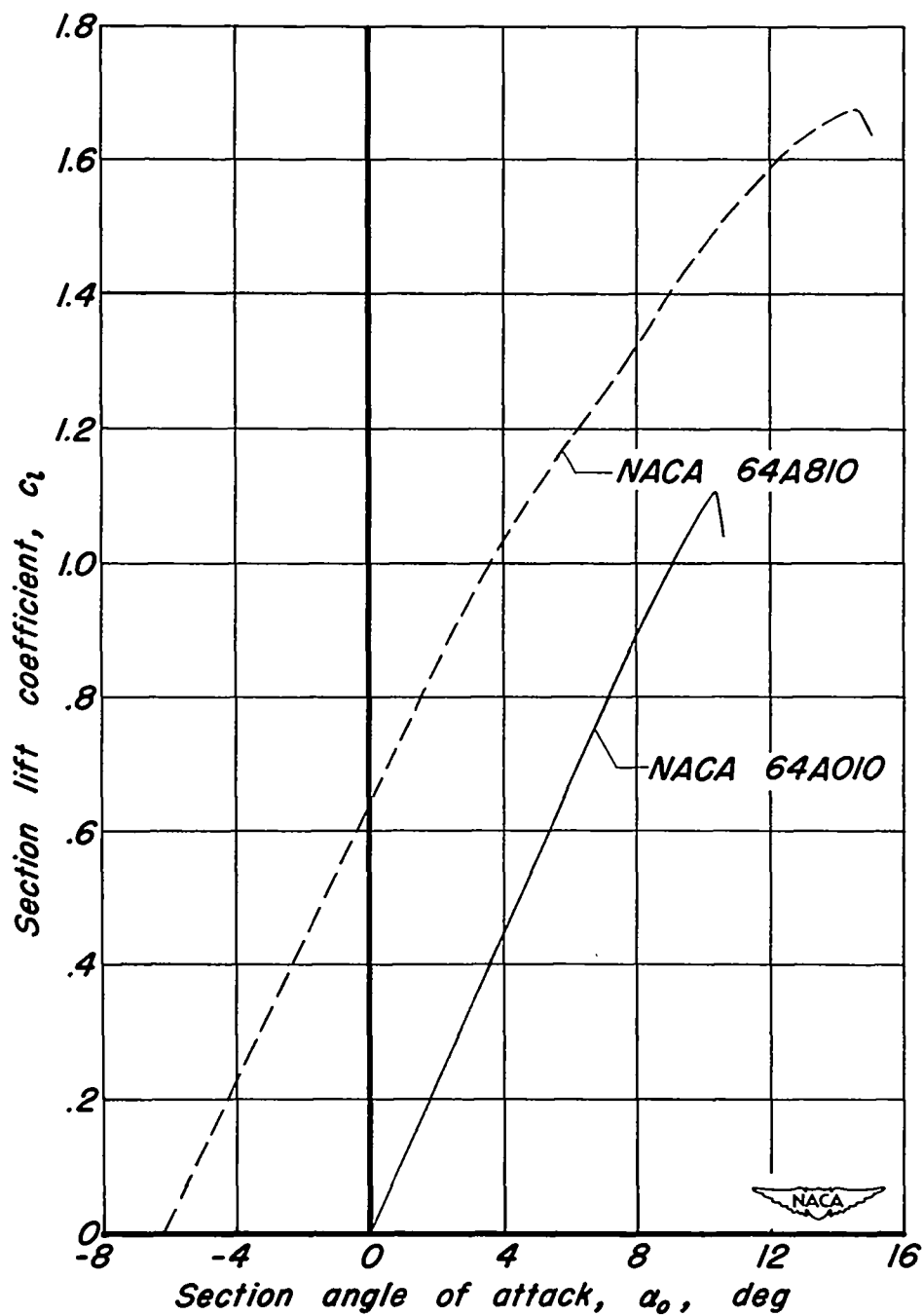
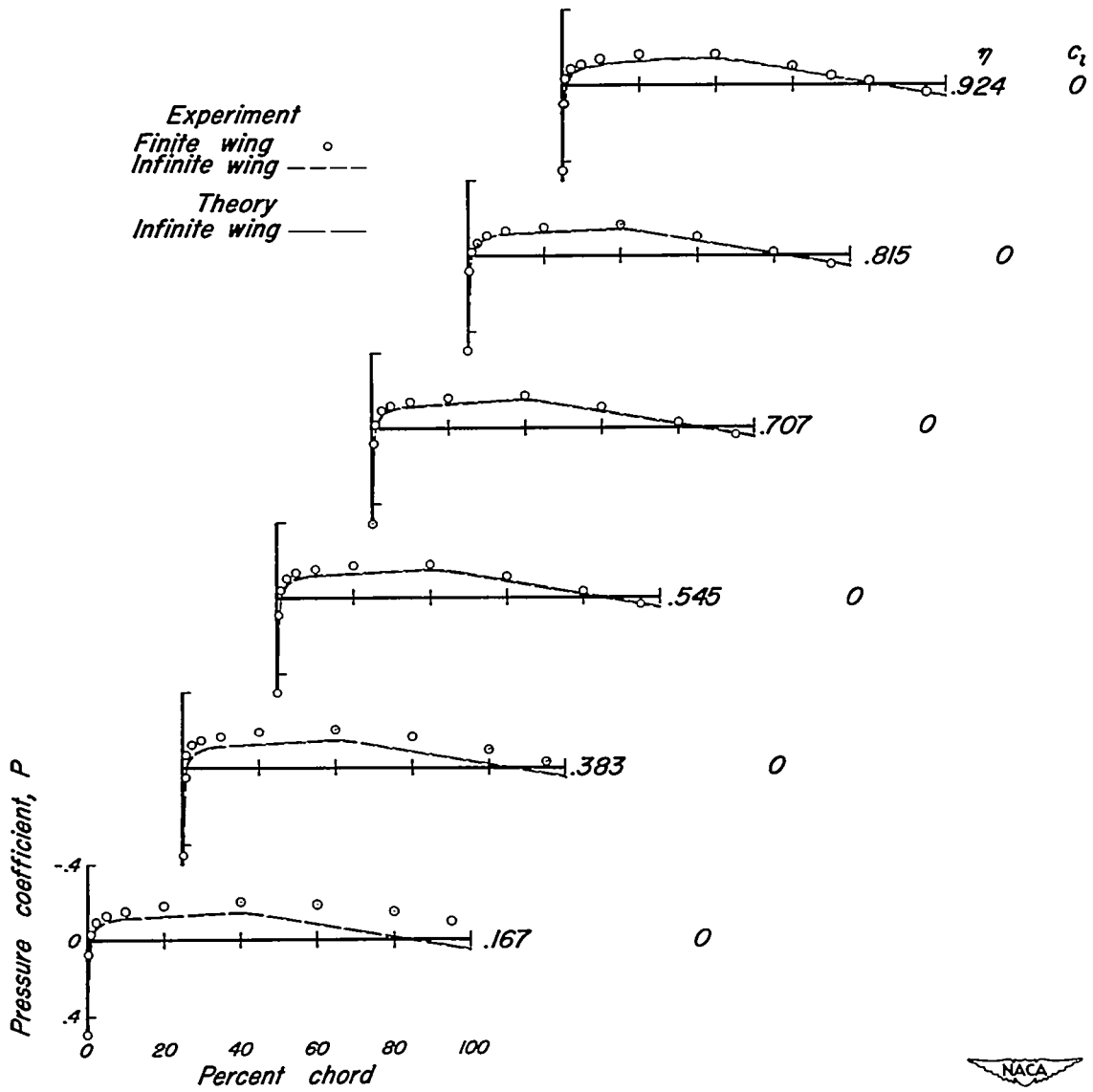
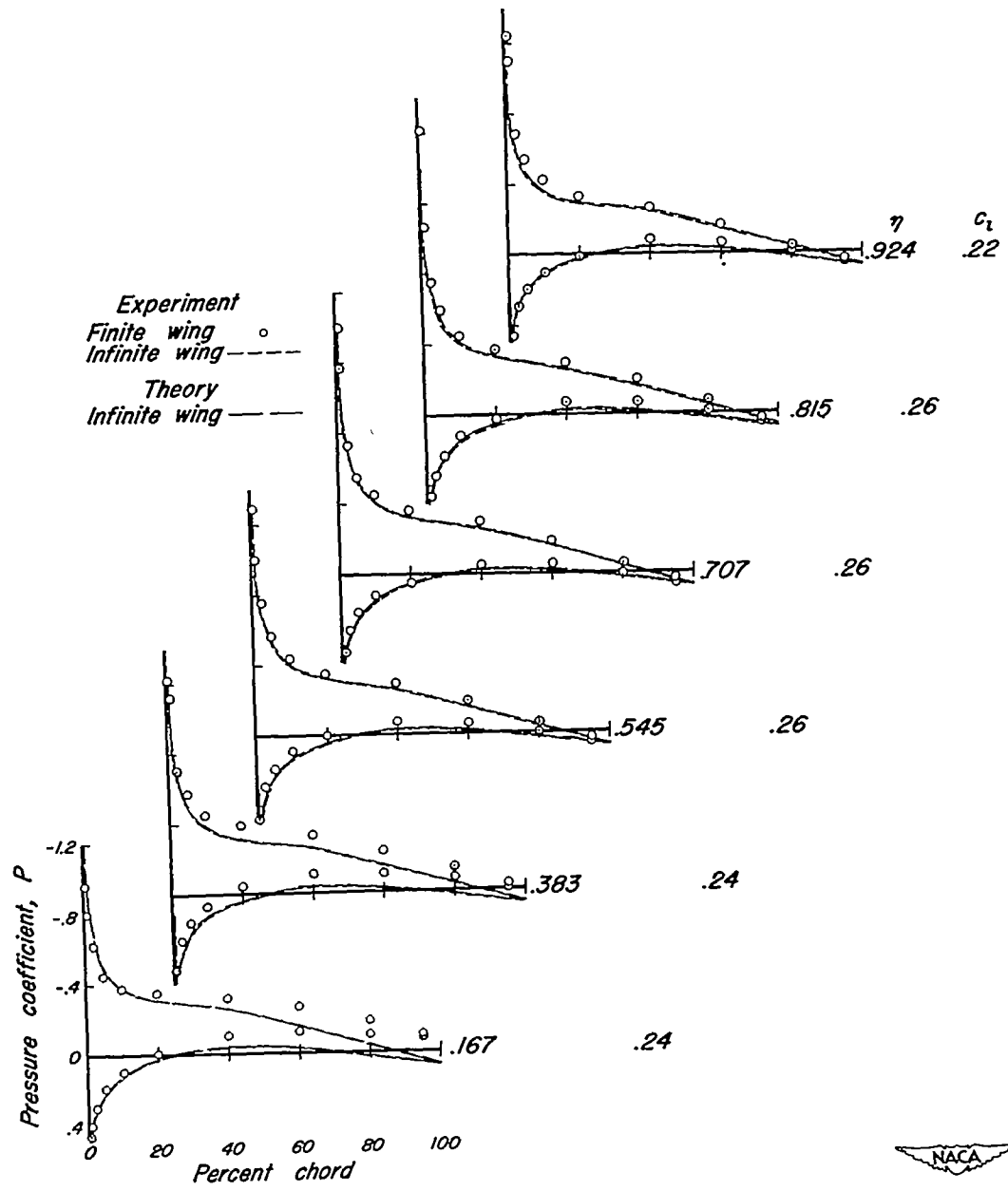


Figure 3.—Lift characteristics of the two airfoil section models.



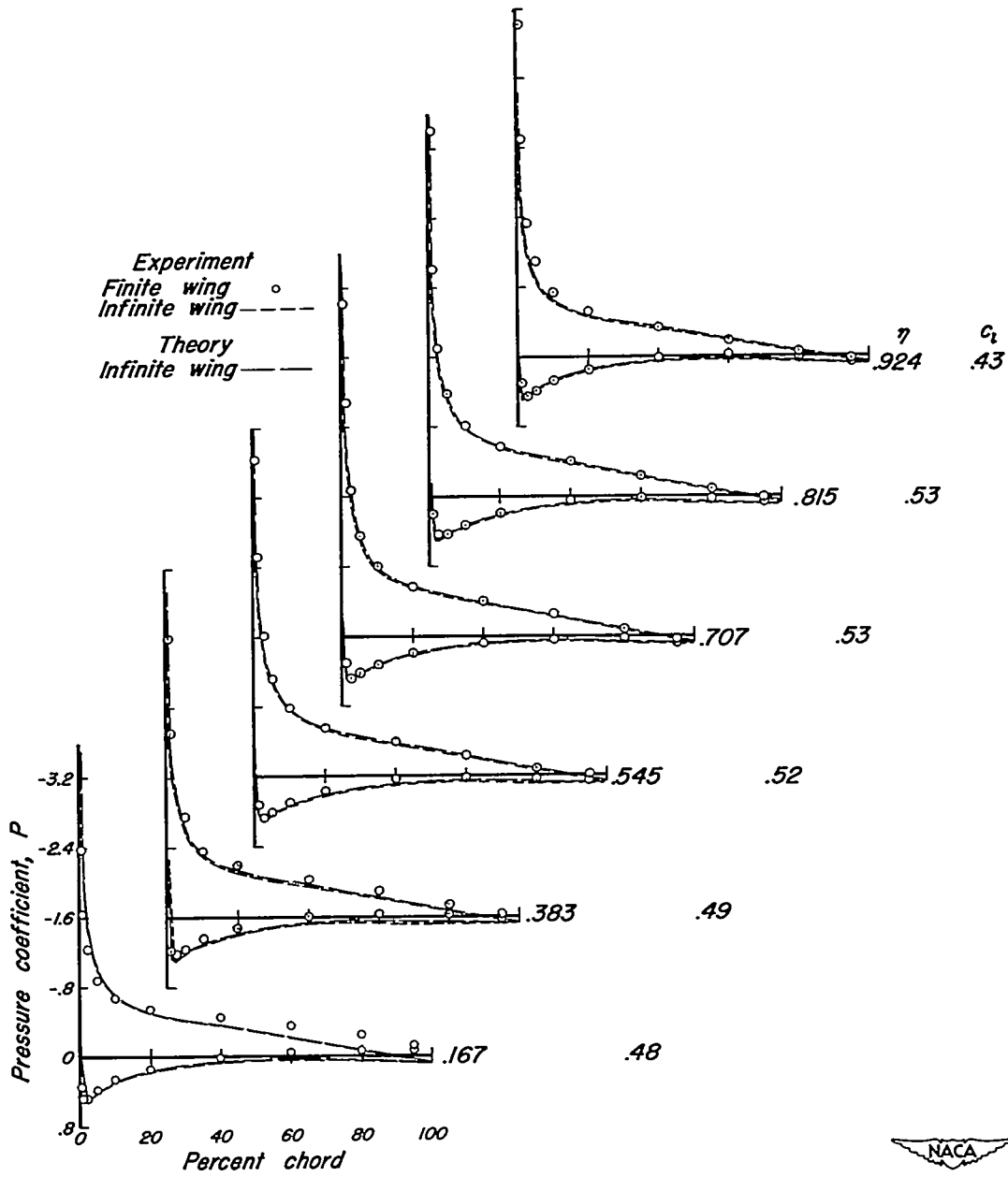
(a)  $C_L, 0$ .

Figure 4.— Comparisons of pressure distributions for six semispan stations of the plain wing with those for the NACA 64A010 section yawed  $45^\circ$  as derived from two-dimensional data and theory.



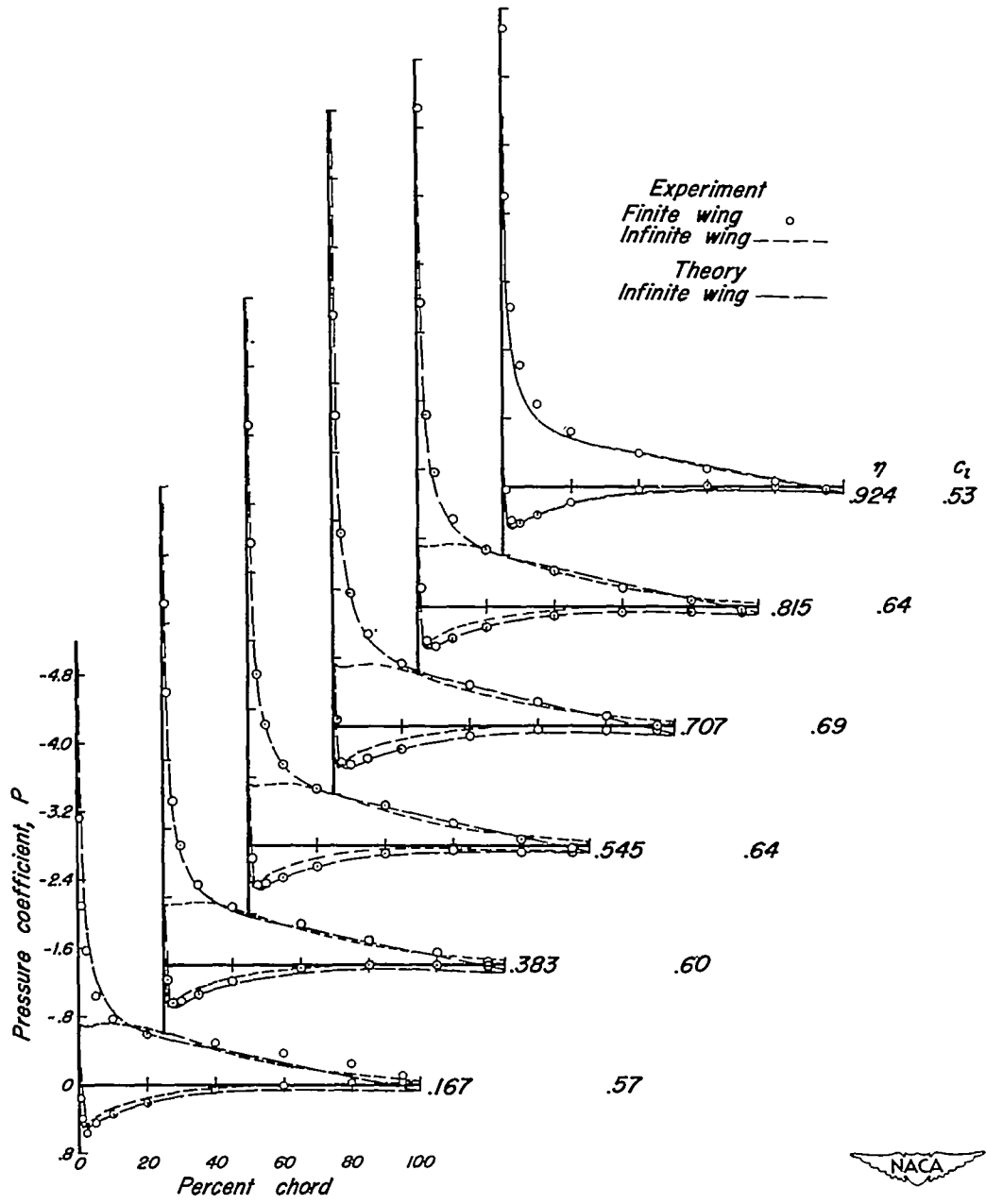
(b)  $C_L$ , 0.24.

Figure 4.—Continued.



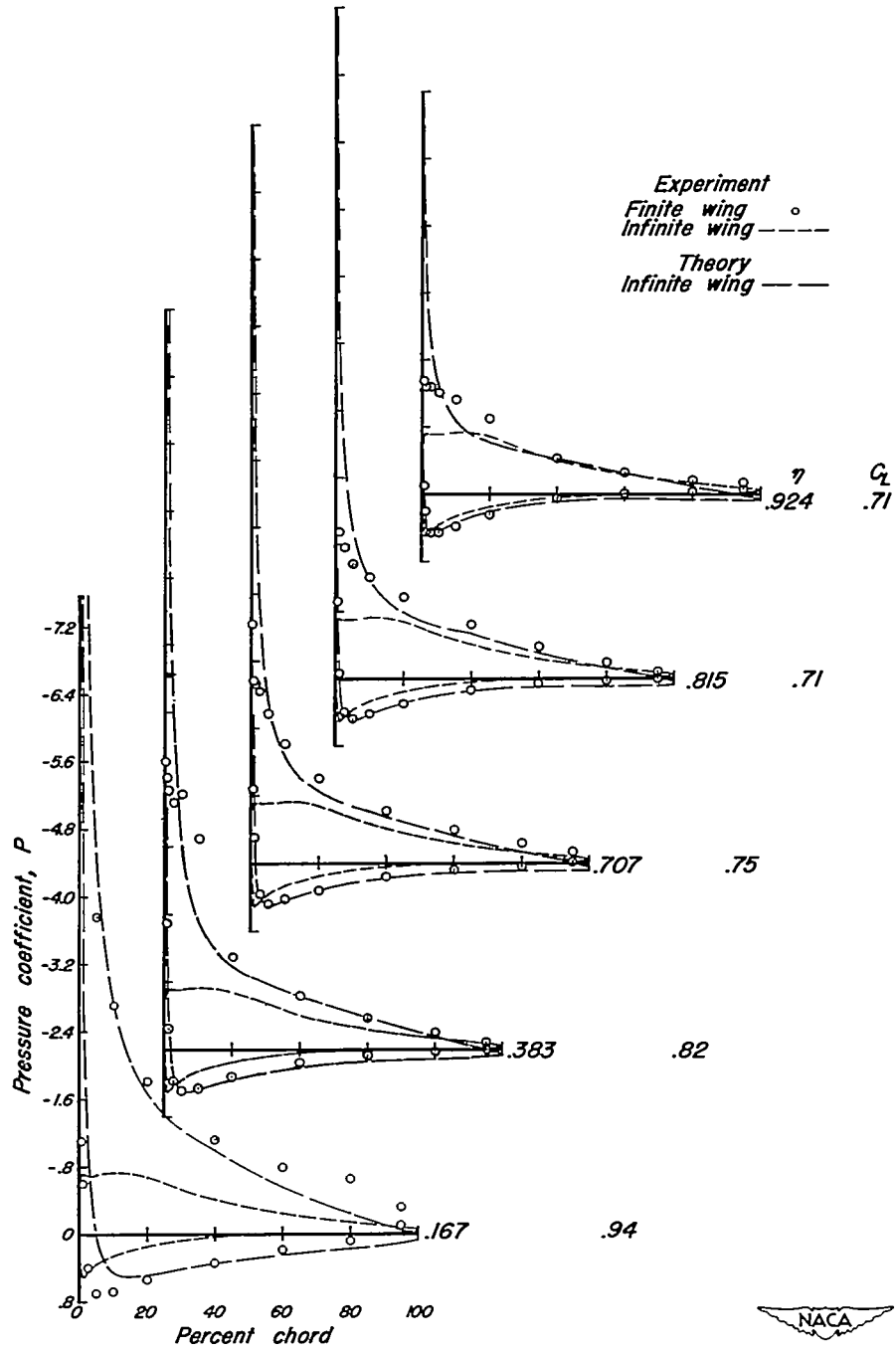
(c)  $C_L$ , 0.48.

Figure 4.—Continued.



(d)  $C_L$ , 0.60.

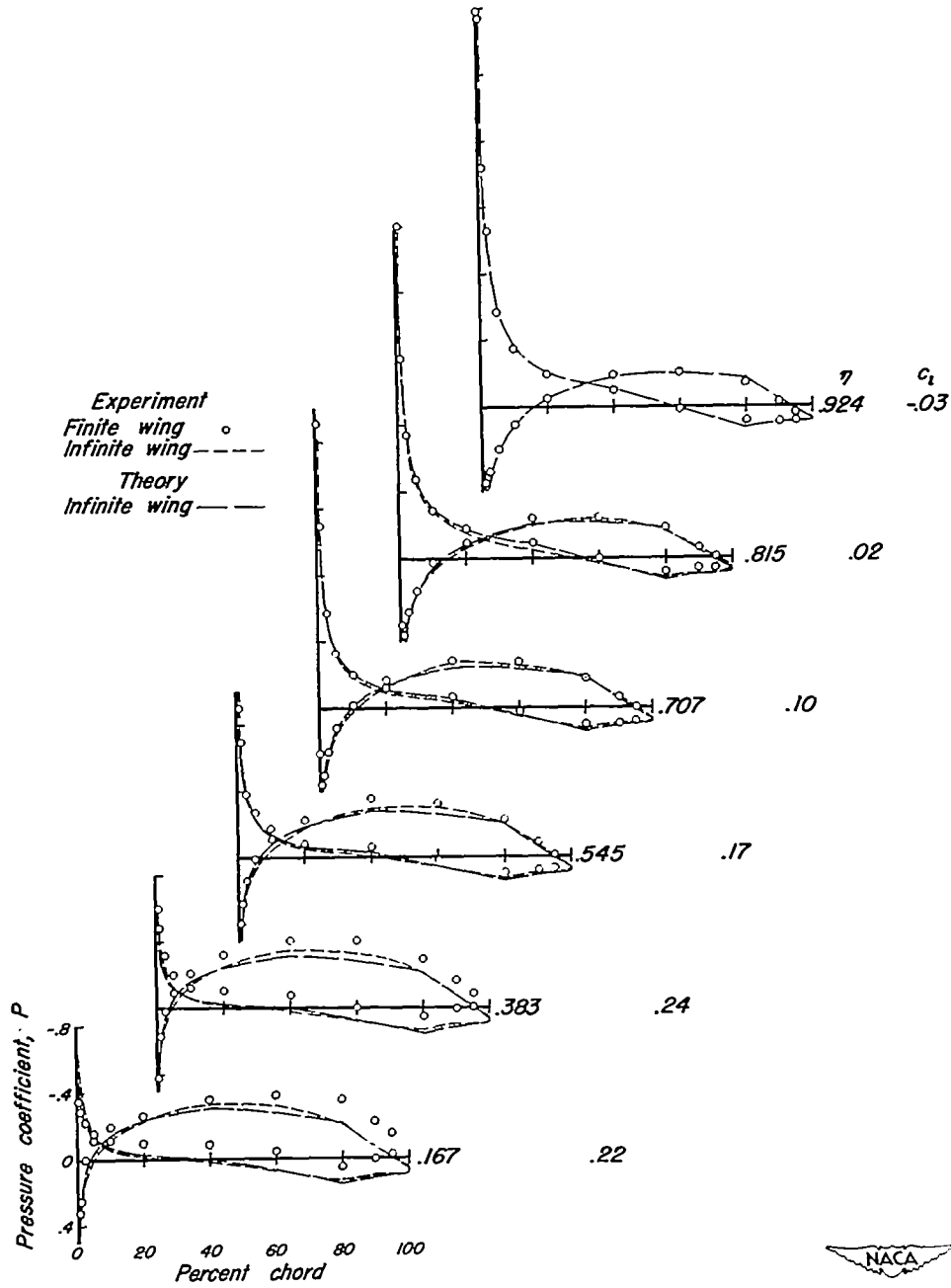
Figure 4.—Continued.



(e)  $C_L$  variable.

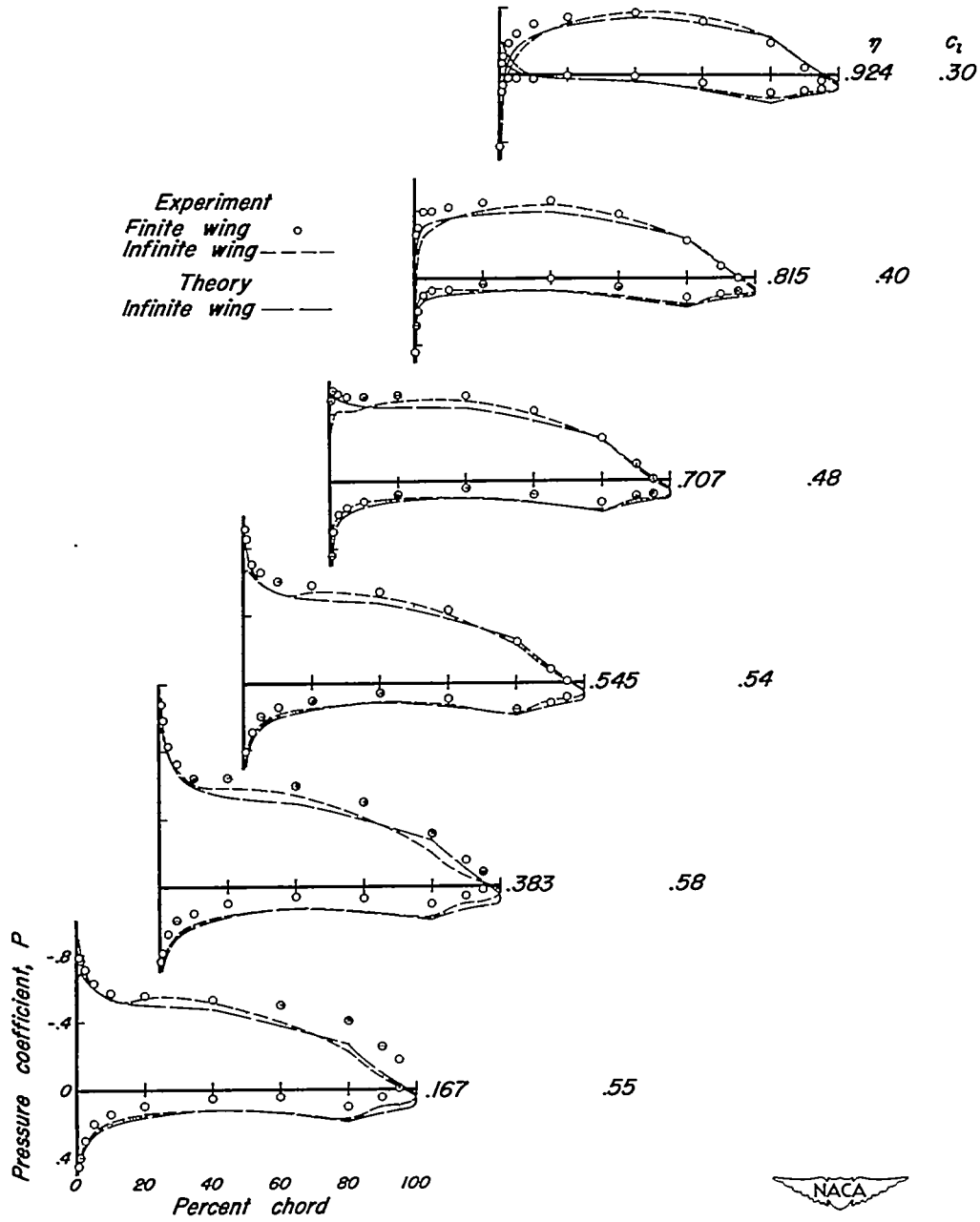
Figure 4.—Concluded.





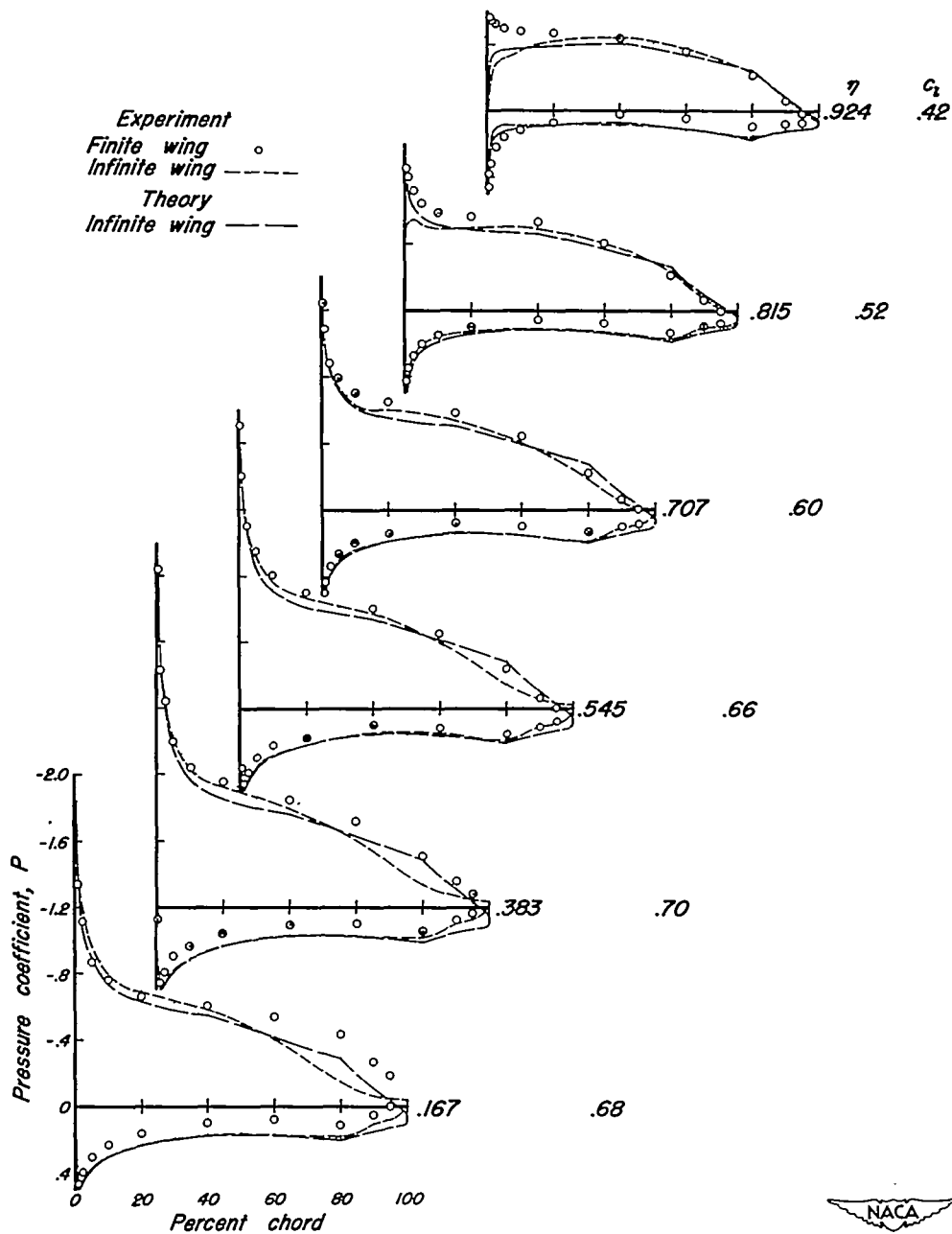
(a)  $C_L$ , 0.15.

Figure 5.— Comparisons of pressure distributions for six semispan stations of the cambered, twisted wing with those for the NACA 64A810 section yawed  $45^\circ$  as derived from two-dimensional data and theory.



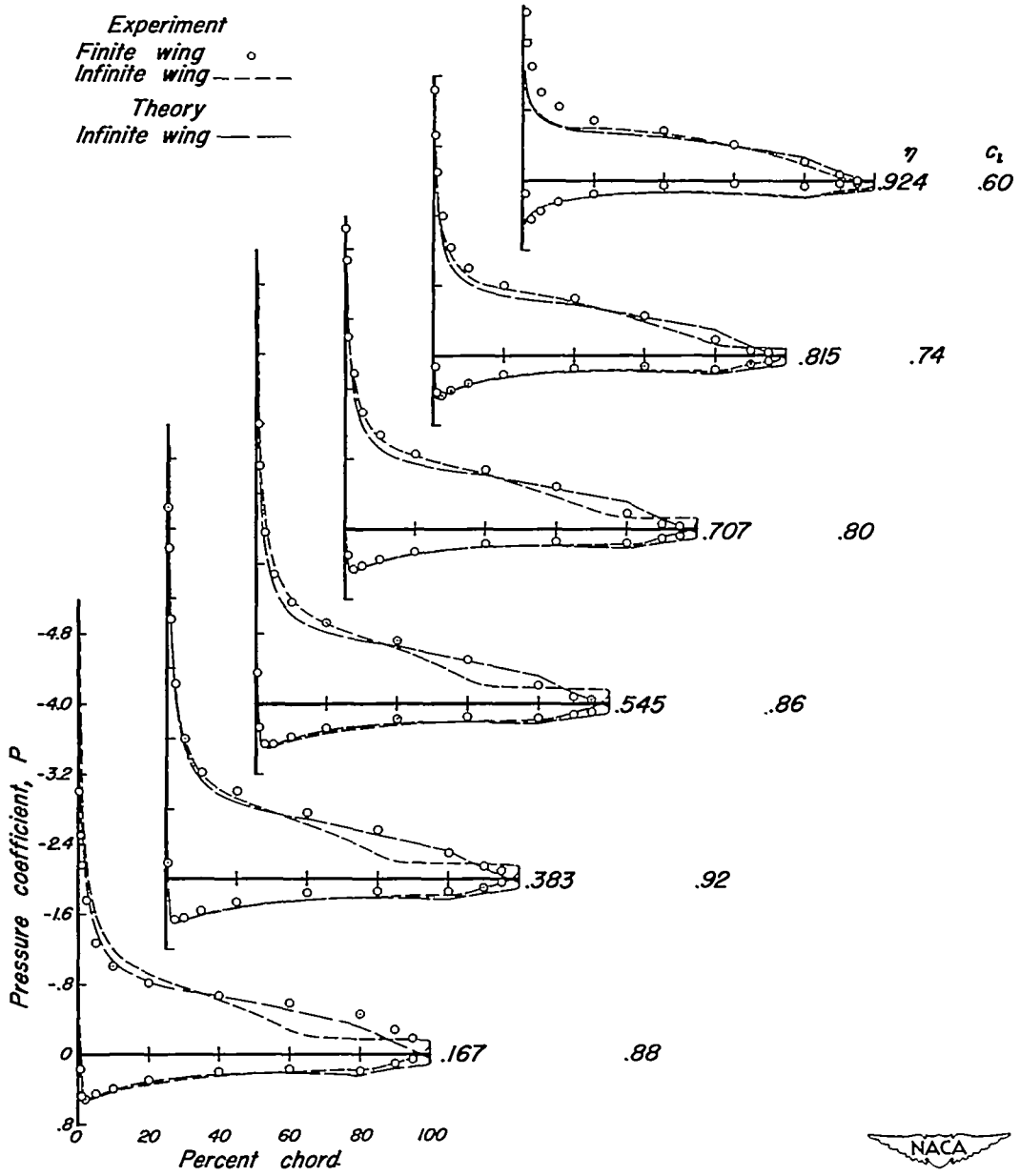
(b)  $C_L, 0.50$ .

Figure 5.—Continued.



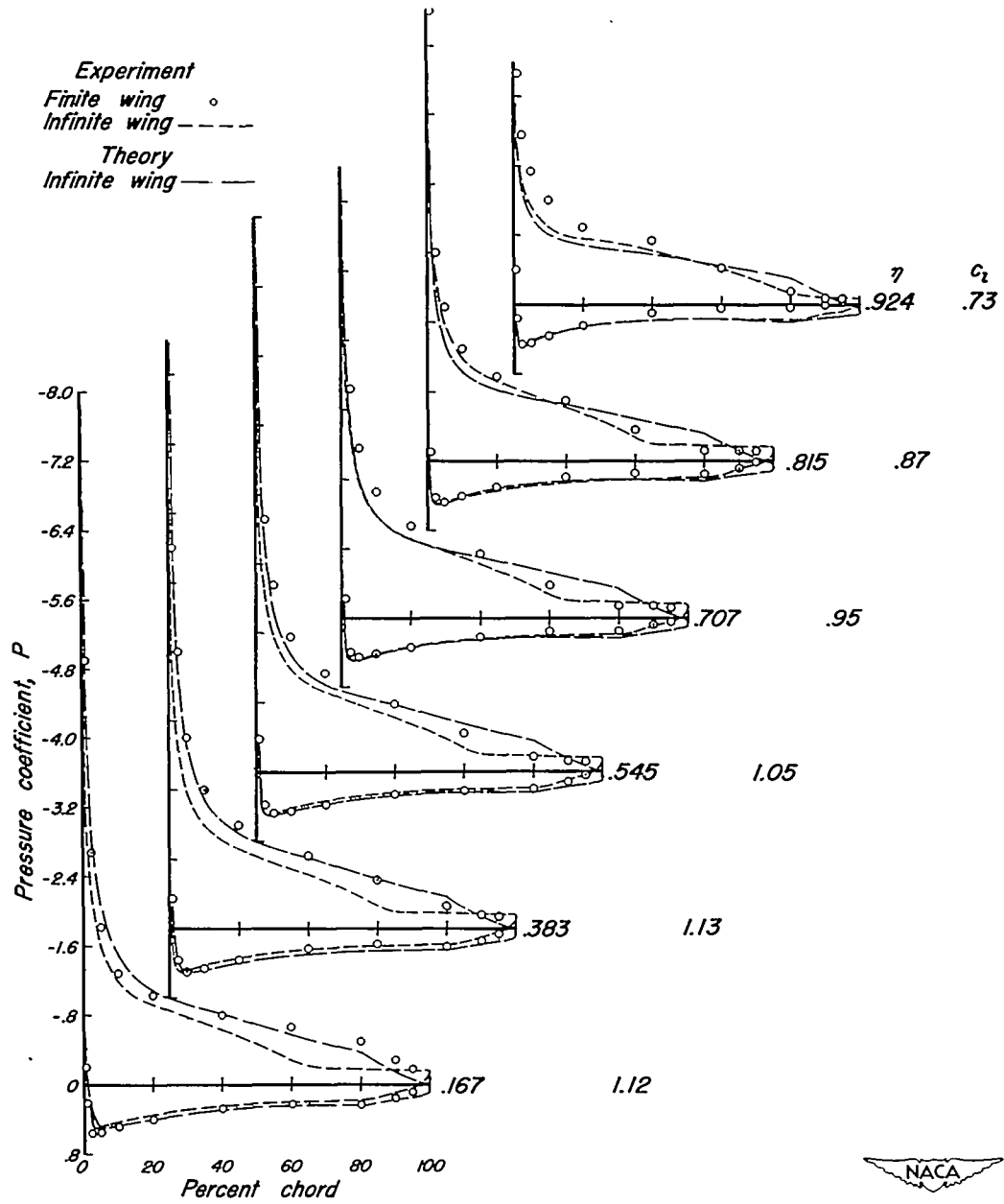
(c)  $C_L$ , 0.62

Figure 5.—Continued.



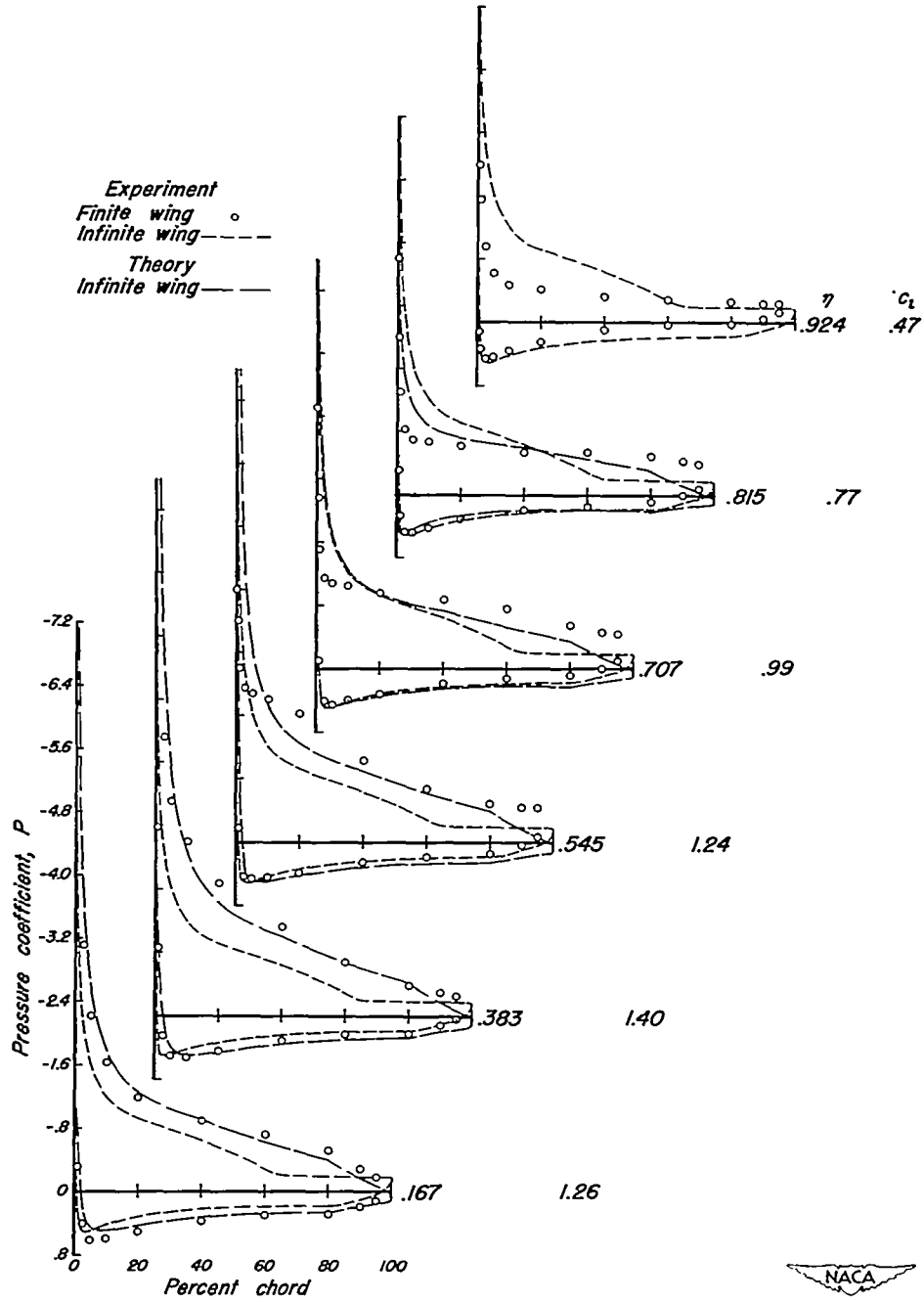
(d)  $C_L$ , 0.83.

Figure 5.—Continued.



(e)  $C_L$ , 1.01.

Figure 5.—Continued.



(f)  $C_L$ , 1.06.

Figure 5.—Concluded.

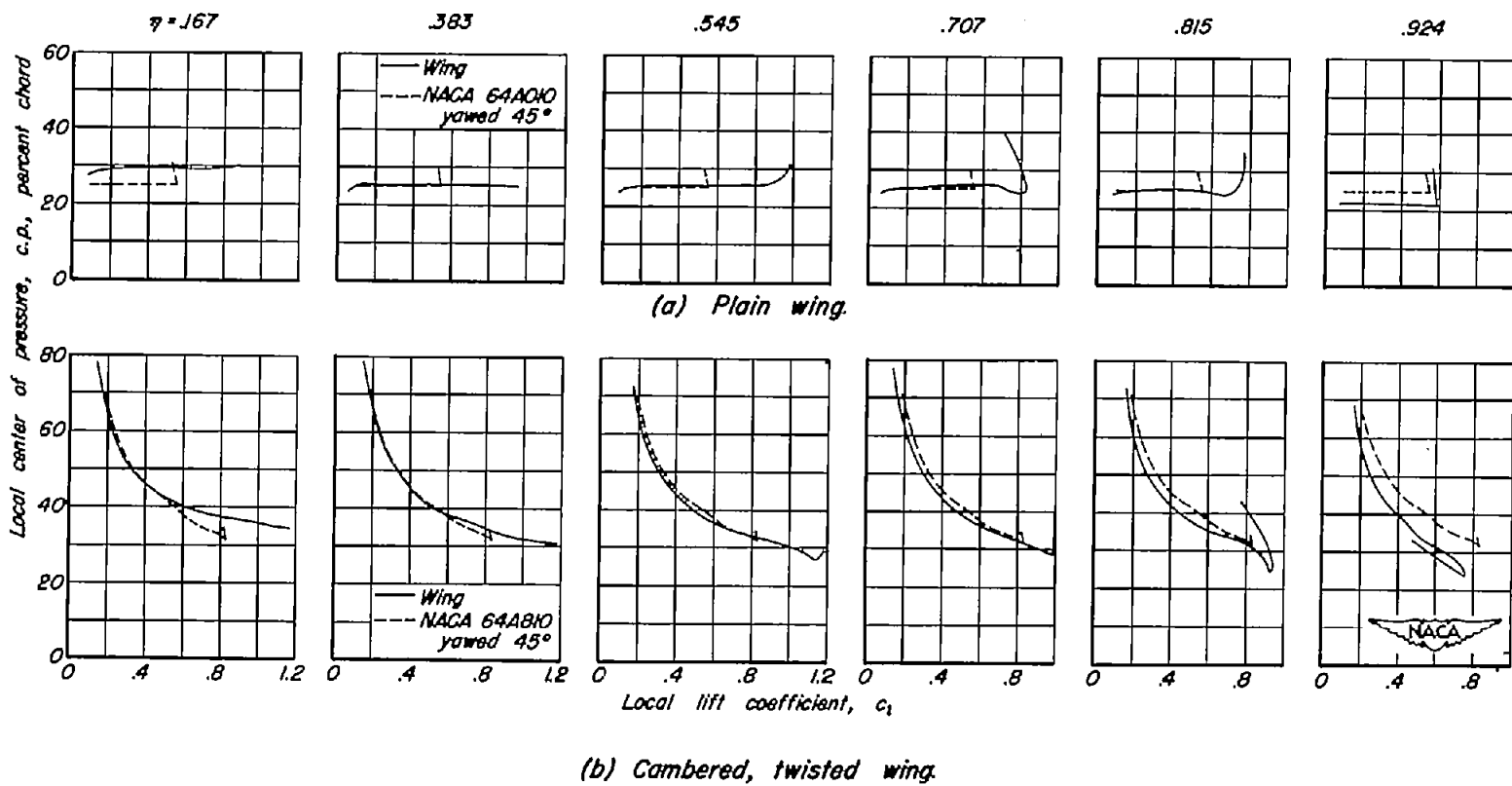
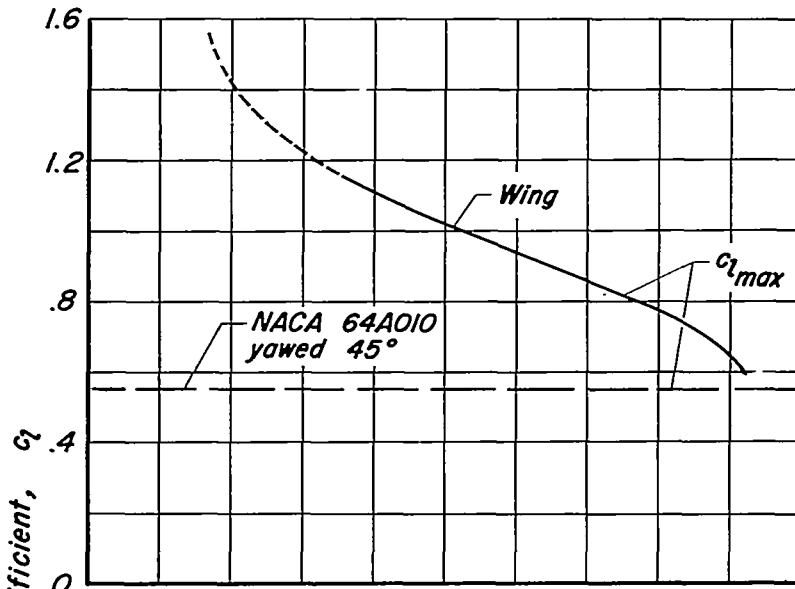
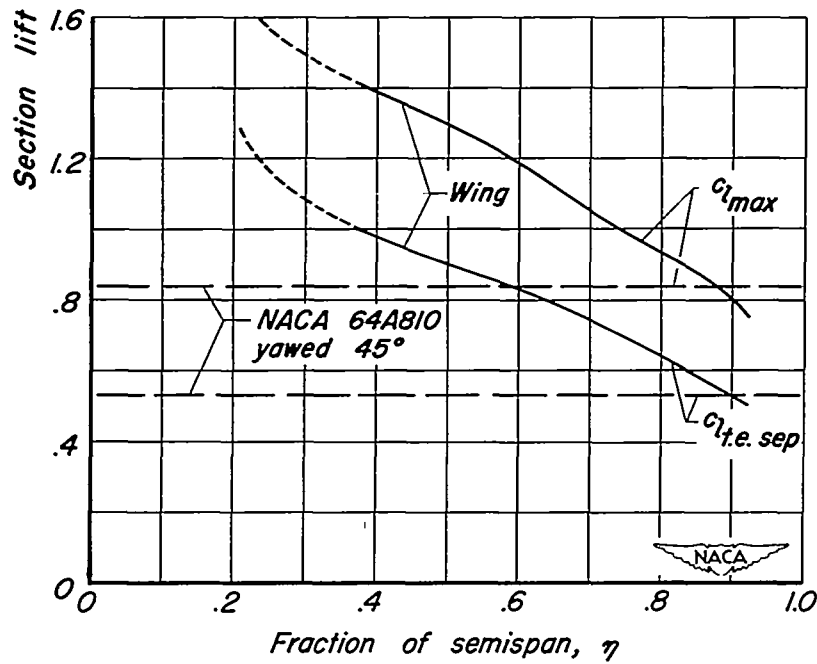


Figure 6.— Comparisons of local centers of pressure on the wing models with those for the corresponding two-dimensional sections.

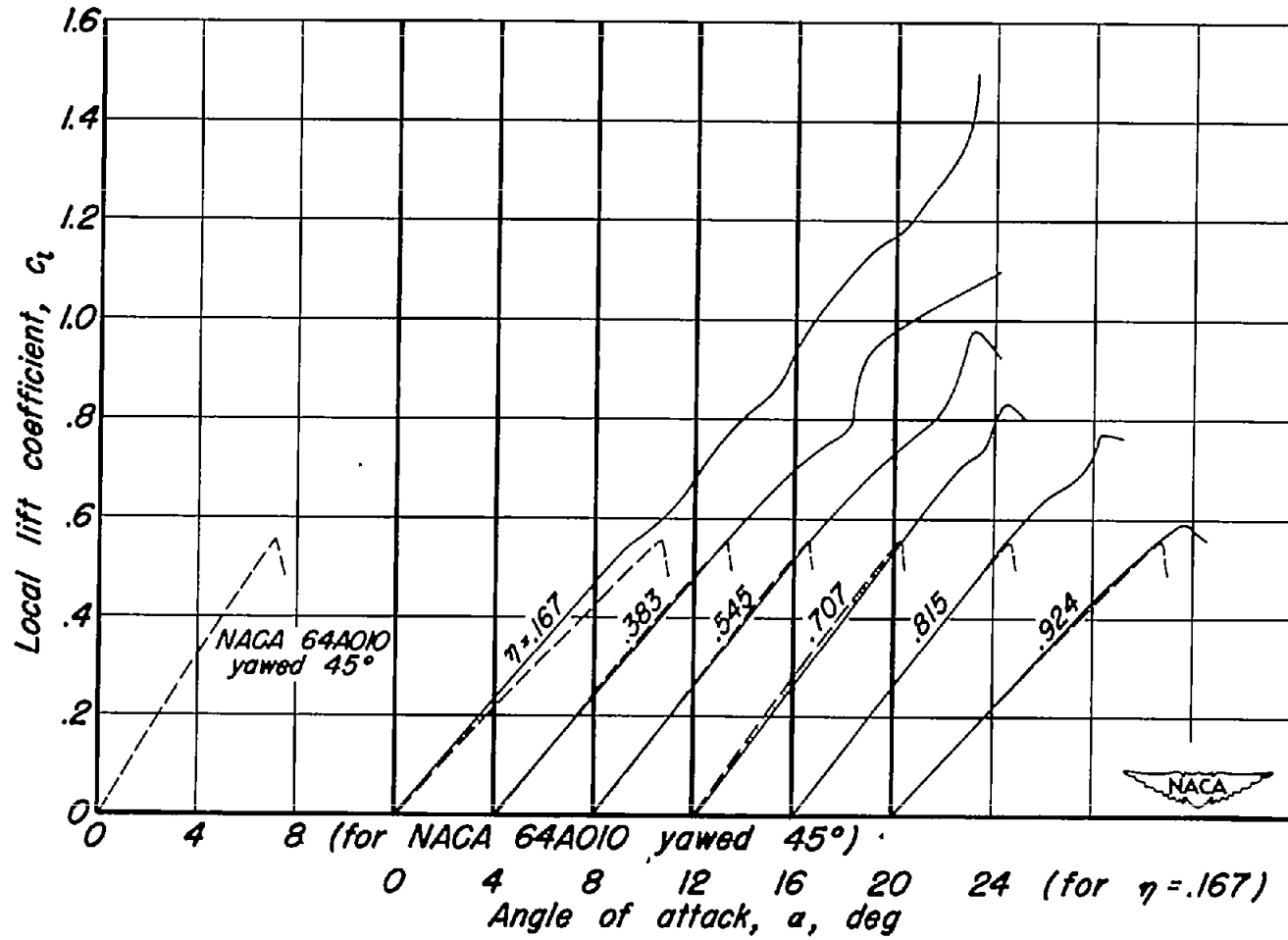


(a) Plain wing.



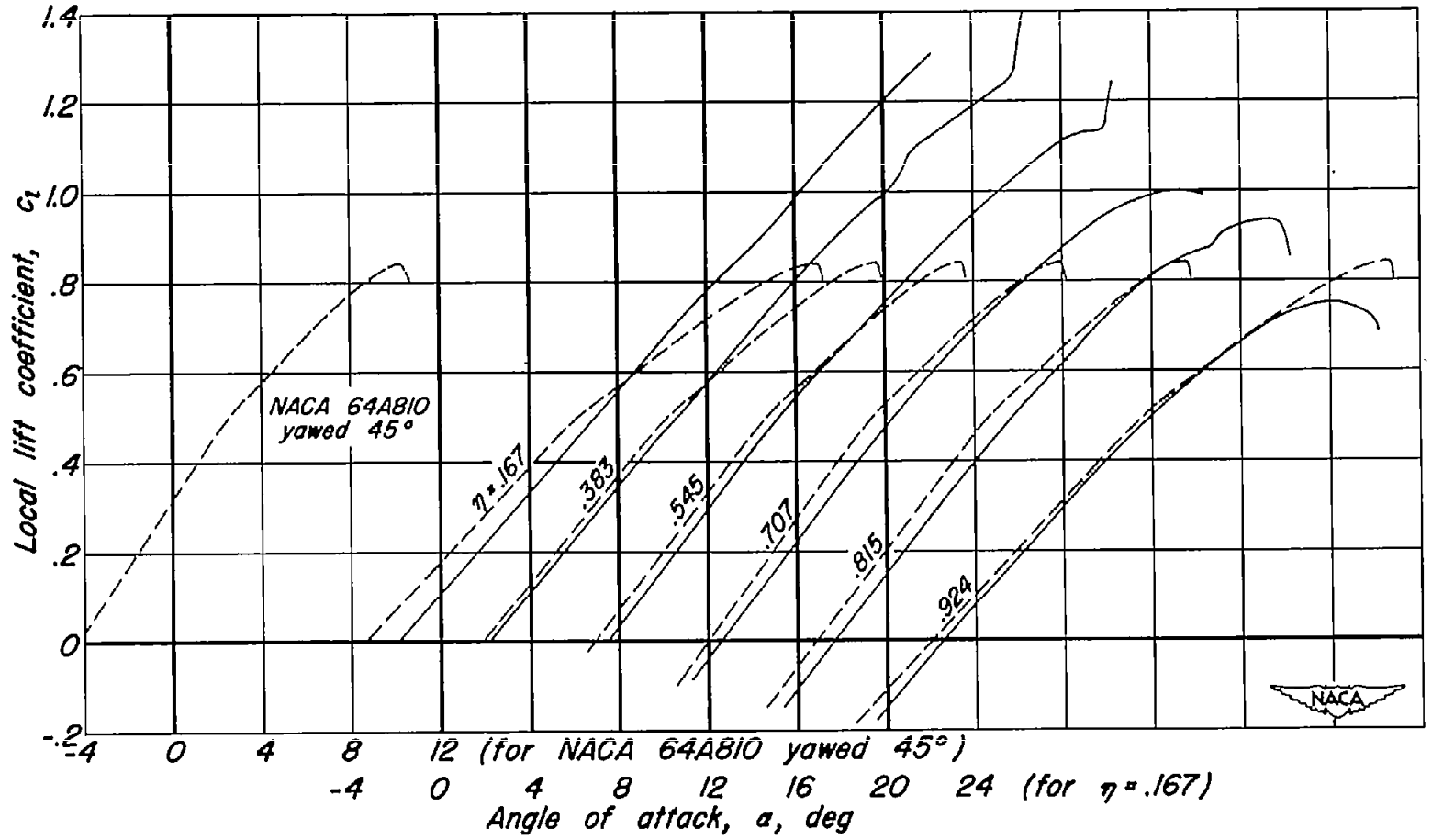
(b) Cambered, twisted wing.

Figure 7.— Variation spanwise of the local lift coefficient for stall on the wing models.



(a) Plain wing.

Figure 8.— Comparisons of local lift curves on the wing models with those derived from two-dimensional data and span loading theory.



(b) Cambered, twisted wing.  
Figure 8.—Concluded.